Open flux estimates in Saturn's magnetosphere during the January 2004 Cassini-HST campaign, and implications for reconnection rates

S. V. Badman,[1] E. J. Bunce,[1] J. T. Clarke,[2] S. W. H. Cowley,[1] J.-C. Gérard,[3] D. Grodent,[3] and S. E. Milan[1]

Received 23 May 2005; revised 23 August 2005; accepted 7 September 2005; published 19 November 2005.

[1] During 8–30 January 2004, a sequence of 68 UV images of Saturn's southern aurora was obtained by the Hubble Space Telescope (HST), coordinated for the first time with measurements of the upstream interplanetary conditions made by the Cassini spacecraft. Using the poleward edge of the observed aurora as a proxy for the open-closed field line boundary, the open flux content of the southern polar region has been estimated. It is found to range from ~15 to ~50 GWb during the interval, such a large variation providing evidence of a significant magnetospheric interaction with the solar wind, in particular with the interplanetary structures associated with corotating interaction regions (CIRs). The open flux is found to decline slowly during a rarefaction region in which the interplanetary magnetic field remained very weak, while decreasing sharply in association with the onset of CIR-related solar wind compressions. Such decreases are indicative of the dominating role of open flux closure in Saturn's tail during these intervals. Increases in open flux are found to occur in the higher-field compression regions after the onsets, and in a following rarefaction region of intermediate field strength. These increases are indicative of the dominating role of open flux production at Saturn's magnetopause during these intervals. The rate of open flux production has been estimated from the upstream interplanetary data using an empirical formula based on experience at Earth, with typical values varying from ~10 kV during the weak-field rarefaction region, to ~200 kV during the strong-field compression. These values have been integrated over time between individual HST image sets to estimate the total open flux produced during these intervals. Comparison with the changes in open flux obtained from the auroral images then allows us to estimate the amount of open flux closed during these intervals, and hence the averaged tail reconnection rates. Intermittent intervals of tail reconnection at rates of ~30–60 kV are inferred in rarefaction regions, while compression regions are characterised by rates of ~100–200 kV, these values representing averages over the ~2-day intervals between HST image sequences. The forms of the aurorae observed are also discussed in relation to the deduced voltage values.

Citation: Badman, S. V., E. J. Bunce, J. T. Clarke, S. W. H. Cowley, J.-C. Gérard, D. Grodent, and S. E. Milan (2005), Open flux estimates in Saturn's magnetosphere during the January 2004 Cassini-HST campaign, and implications for reconnection rates, *J. Geophys. Res.*, *110*, A11216, doi:10.1029/2005JA011240.

1. Introduction

[2] The first indications that ultraviolet (UV) auroral emissions occur in Saturn's polar regions were obtained by the Pioneer-11 spacecraft during its fly-by in 1979 [*Judge et al.*, 1980], and remotely by the IUE spacecraft [*Clarke et al.*, 1981; *McGrath and Clarke*, 1992]. The first unambiguous detections were made by the two Voyager spacecraft in 1980 and 1981 [*Broadfoot et al.*, 1981; *Sandel and Broadfoot*, 1981; *Sandel et al.*, 1982; *Shemansky and Ajello*, 1983]. Subsequently, a number of individual images of Saturn's polar aurorae have been obtained using the Hubble Space Telescope (HST), showing them typically to form relatively narrow bands around the northern and southern magnetic poles, often brighter at dawn than at dusk, lying at co-latitudes between ~10° and ~20° [*Gérard et al.*, 1995, 2004; *Trauger et al.*, 1998; *Cowley et al.*, 2004a; *Prangé et al.*, 2004]. The HST images have also revealed considerable changes in location and intensity, the brightness varying from below few kR detection thresholds to peaks of over ~100 kR. This variability contrasts sharply with the relative stability of Jupiter's 'main oval' aurorae, which remain essentially fixed in location relative to the magnetic pole, and vary in overall intensity typically by

[1]Department of Physics and Astronomy, University of Leicester, Leicester, UK.
[2]Department of Astronomy, Boston University, Boston, Massachusetts, USA.
[3]LPAP, Université de Liège, Liège, Belgium.

0148-0227/05/2005JA011240$09.00

factors of only two or three [e.g., *Clarke et al.*, 1998; *Prangé et al.*, 1998; *Grodent et al.*, 2003].

[3] Two basic theoretical ideas have been proposed to account for such circumpolar bands of UV emission. The first is that the auroral field lines map into the interior of the magnetosphere, and are associated with the field-aligned current system required to maintain partial corotation of the magnetospheric plasma, due to plasma particle pick-up from interior neutral sources and to outward radial diffusion [e.g., *Hill*, 1979, 2001; *Vasyliunas*, 1983]. Using a realistic model of the field and flow in Jupiter's magnetosphere, *Cowley and Bunce* [2001] showed that this current system, specifically the region of upward current carried by downward-accelerated precipitating magnetospheric electrons, can account quantitatively for the location and intensity of Jupiter's 'main oval' aurorae. The intensity of such aurorae can be modulated by solar wind-induced compressions and expansions of the magnetosphere which change the angular velocity of the plasma through angular momentum conservation [e.g., *Southwood and Kivelson*, 2001; *Cowley and Bunce*, 2003a]. However, recent calculations show that when ionospheric conductivity feed-back effects are included, the upward current region becomes concentrated into the inner part of the system where it is more insulated from solar wind effects [*Nichols and Cowley*, 2004], thus possibly accounting for the relative stability of these emissions at Jupiter. *Cowley and Bunce* [2003b] investigated whether a similar current system could also be responsible for the UV emissions at Saturn, using models of the magnetospheric magnetic field and plasma angular velocity based on Voyager observations. In this case, however, they found that the upward currents are both too weak and lie at too low a latitude to account for Saturn's UV auroral oval.

[4] The second possibility is that the aurorae are produced by field-aligned currents and hot plasma precipitation associated with the solar wind-magnetosphere interaction, principally the Dungey cycle flow excited by reconnection at the magnetopause and in the tail [*Dungey*, 1961]. This is the main process that controls magnetospheric plasma dynamics at Earth (see e.g. the recent review by *Cowley et al.* [2003]), resulting in highly variable auroral emissions that respond strongly to conditions in the interplanetary medium. In this case the aurorae generally lie at and equatorward of the boundary between open and closed field lines, which expands and contracts with reconnection events and the associated varying amount of open flux in the system [e.g., *Milan et al.*, 2003, 2004]. Recently, the effect of Dungey-cycle processes on the rapidly-rotating magnetosphere of Saturn has been considered by *Cowley et al.* [2004a, 2004b], who showed that a ring of upward field-aligned current strong enough to produce bright aurorae should occur at the open-closed field line boundary, with stronger currents and brighter aurorae occurring at dawn compared with dusk when the Dungey-cycle is active. In addition, hot plasma production in tail reconnection events, followed by rotation around the outer magnetosphere due to ionospheric coupling, should also result in the formation of 'diffuse' auroral forms which spiral around the open-closed field line boundary from midnight via dawn [*Cowley et al.*, 2005], thus matching a common auroral morphology at Saturn [*Gérard et al.*, 2004]. Overall, these studies strongly suggest that the auroral oval at Saturn is associated with the solar wind-magnetosphere interaction, and is located in the vicinity of the open-closed field line boundary. This conclusion is also in accord with estimates of the boundary location based on in situ Voyager magnetic field measurements [*Ness et al.*, 1981; *Cowley et al.*, 2004b].

[5] In January 2004 an unprecedented sequence of UV images of Saturn's southern aurora was obtained by the HST over a three week interval [*Clarke et al.*, 2005; *Grodent et al.*, 2005], in coordination with observations of the interplanetary medium upstream from Saturn by the Cassini spacecraft en route to orbit insertion at the planet [*Crary et al.*, 2005; *Bunce et al.*, 2005b]. These images record a substantial variability in the auroral emissions over the interval, in line with the above discussion, responding strongly to recurrent corotating interaction region (CIR) compressions in the heliosphere. Specifically, following the arrival at Saturn of solar wind compressions in which the dynamic pressure (principally the density) and the magnetic field strength of the solar wind are strongly enhanced, the auroral emission expanded significantly poleward in the nightside and dawn sector, before forming a bright spiral structure extending from dawn to later local times. *Cowley et al.* [2005] proposed that these events are formed by bursts of tail reconnection excited by the sudden magnetospheric compression produced by the arrival of the leading ('forward') shock of the CIR compression region. Similar shock-induced auroral events are occasionally observed at Earth involving rapid closure of a significant fraction of the open magnetic flux in the tail [e.g., *Boudouridis et al.*, 2003, 2004; *Milan et al.*, 2004; *Meurant et al.*, 2004]. The exact physics leading to the onset or enhancement of tail reconnection under these circumstances has not yet been determined in detail. We note, however, that compression of the magnetosphere will both reduce the thickness of the plasma sheet while simultaneously increasing the cross-tail current it has to carry (through the increased field strength in the tail lobes). Both effects require an increase in the plasma sheet current density, which may lead to instability. Formally, compression of the magnetosphere is related to the combined action of the dynamic, thermal, and magnetic pressures of the solar wind plasma. However, for a highly super-magnetosonic flow such as the solar wind, the dynamic pressure is by far the dominant component, such that we suppose the above auroral effects relate principally to this parameter. We also note that *Desch* [1982] and *Desch and Rucker* [1983] have previously used Voyager data to show that bursts of high-intensity Saturn kilometric radiation (SKR) are strongly correlated with the dynamic pressure of the upstream solar wind. We therefore suggest that these radio bursts are directly connected with CIR-related auroral events as described above and note that such bursts were observed by the Cassini spacecraft in association with the CIR-related auroral events in January 2004 [*Kurth et al.*, 2005]. While the dynamic pressure of the solar wind (principally through the density) is then a key parameter in Saturn's magnetospheric dynamics, we also point out that due to the frozen-in nature of the flow, the magnetic field

strength forms a rough but useful proxy, as is demonstrated in the Cassini data presented below.

[6] Based on the above discussion and that of *Cowley et al.* [2004a, 2004b, 2005], it seems reasonable to suppose that the poleward boundary of Saturn's UV aurorae observed by the HST lies close to the boundary between open and closed field lines, and expands and contracts with episodes of magnetopause and tail reconnection. This assumption will be taken as the working hypothesis in this paper. In this case, then, we can use the HST images obtained in January 2004 to estimate the variations in open flux present in Saturn's magnetosphere over that interval. The overall change in open flux that occurs during an interval is given by the difference in the amount of open flux that is created at the magnetopause, and that which is destroyed by reconnection in the tail. In a recent paper, *Jackman et al.* [2004] have proposed a formula for the magnetopause reconnection rate at Saturn in terms of the upstream interplanetary field and plasma parameters, based on empirical data obtained at Earth. If we then employ this formula to estimate the open flux produced during an interval, we can also infer from the overall open flux change the amount of open flux that has been closed during the interval, and hence the averaged tail reconnection rate. In this paper we thus combine open flux estimates derived from HST images with concurrent estimates of open flux production determined from Cassini measurements of upstream interplanetary parameters, to discuss magnetopause and tail reconnection rates and overall magnetospheric dynamics at Saturn during the January 2004 Cassini-HST campaign. We also discuss our conclusions in relation to the nature of the auroral forms which were observed. We begin in the next section by providing a brief overview of the Cassini-HST campaign data, together with a discussion showing how the open flux estimates were obtained from the images.

2. Cassini Observations, HST Images, and Open Flux Estimates

2.1. Overview of the January 2004 HST-Cassini Campaign Data

[7] The structure of the interplanetary medium in the vicinity of Saturn's orbit during Cassini's approach to the planet, encompassing the interval of interest here, has been discussed by *Jackman et al.* [2004]. Using interplanetary magnetic field (IMF) data obtained by Cassini over a 6.5-month interval encompassing eight solar rotations at the spacecraft, they showed that the structure of the heliosphere was consistent with a tilted solar dipole field, as expected for the declining phase of the solar cycle. Specifically, the IMF consisted of two sectors per solar rotation, with heliospheric current sheet (HCS) crossings embedded within few-day high-field regions associated with corotating interaction region (CIR) compressions, separated by several-day low-field regions associated with solar wind rarefactions. This structuring is evident in the IMF and solar wind data obtained by Cassini during the January 2004 HST imaging campaign, presented here in Figure 1 for the interval days 1–31 of 2004 [*Crary et al.*, 2005; *Bunce et al.*, 2005b]. The first three panels of the figure show the IMF components in RTN coordinates, while the fourth panel shows the total field strength. RTN is a right-handed spherical polar system referenced to the Sun's spin axis, with B_R directed radially outward from the Sun, B_T azimuthal in the direction of planetary motion, and B_N normal to the other two components, that is, positive northwards from the equatorial plane. The next three panels display the solar wind velocity (v_{SW}), density (n), and dynamic pressure (P_{SW}), respectively, where the dynamic pressure is calculated from

$$P_{SW} = 1.92 \times 10^{-6} \times n\left(\mathrm{cm}^{-3}\right) v_{SW}\left(\mathrm{km\ s}^{-1}\right)^2 \mathrm{nPa}, \qquad (1)$$

assuming that the solar wind is composed of protons and alpha particles in the ratio 19:1. The final panel shows the magnetopause reconnection voltage (open flux production rate) estimated using the algorithm of *Jackman et al.* [2004], which will be discussed in section 3.2 below.

[8] Although plasma data are not available at the beginning of the interval shown in Figure 1, it is evident from the field magnitude data that the interval began with a 'major' CIR-related compression region during days 1–6, with field magnitudes typically ~1–2 nT. Following this, a rarefaction region of very weak fields, ~0.1 nT or less, was observed, associated with slowly falling solar wind speeds and densities ~0.01 cm^{-3} or less. This interval was ended by the arrival of a 'minor' CIR compression on day 15, within which a HCS crossing was embedded, as indicated by the B_T polarity reversal from negative to positive. Within the compression the field strength increased to ~0.2–0.5 nT, while the solar wind speed increased to ~530 km s^{-1} and the density to ~0.1 cm^{-3}. Following this compression, a rarefaction region of intermediate characteristics was then observed during days 19–25, with IMF strengths typically ~0.3 nT, and solar wind densities in the range ~0.01–0.04 cm^{-3}. A third compression then began at the spacecraft on day 25, corresponding to the re-appearance of the 'major' compression observed at the beginning of the interval after one solar rotation. A traversal of the HCS from B_T positive to negative occurred on day 26. This compression lasted until almost the end of the interval considered here, characterised by IMF strengths ~1–2 nT, increased solar wind speeds up to 630 km s^{-1}, and densities ~0.03–0.1 cm^{-3}. Here we note that it is evident from the restricted interval when both plasma and field magnitude data are available, that the field magnitude forms a rough proxy for the dynamic pressure as suggested above. Therefore we can infer the nature and timings of structures in the solar wind even when plasma data are unavailable.

[9] These interplanetary conditions form the back-drop to the HST auroral observations analysed here. The approximate timing of the HST observations relative to the Cassini data are indicated by the vertical dashed lines in Figure 1, where account has been taken both of the propagation delay of the solar wind from Cassini to Saturn, and the light travel time from Saturn to the HST (68 min). During this interval Cassini was located near the ecliptic ~0.2 AU upstream of Saturn, and ~0.5 AU off the Sun-planet line towards dawn. Using an average solar wind speed of 500 km s^{-1}, the radial solar wind propagation delay from the spacecraft to the planet is thus estimated as ~17 h. This time is uncertain to within a few hours, however, due to possible non-radial

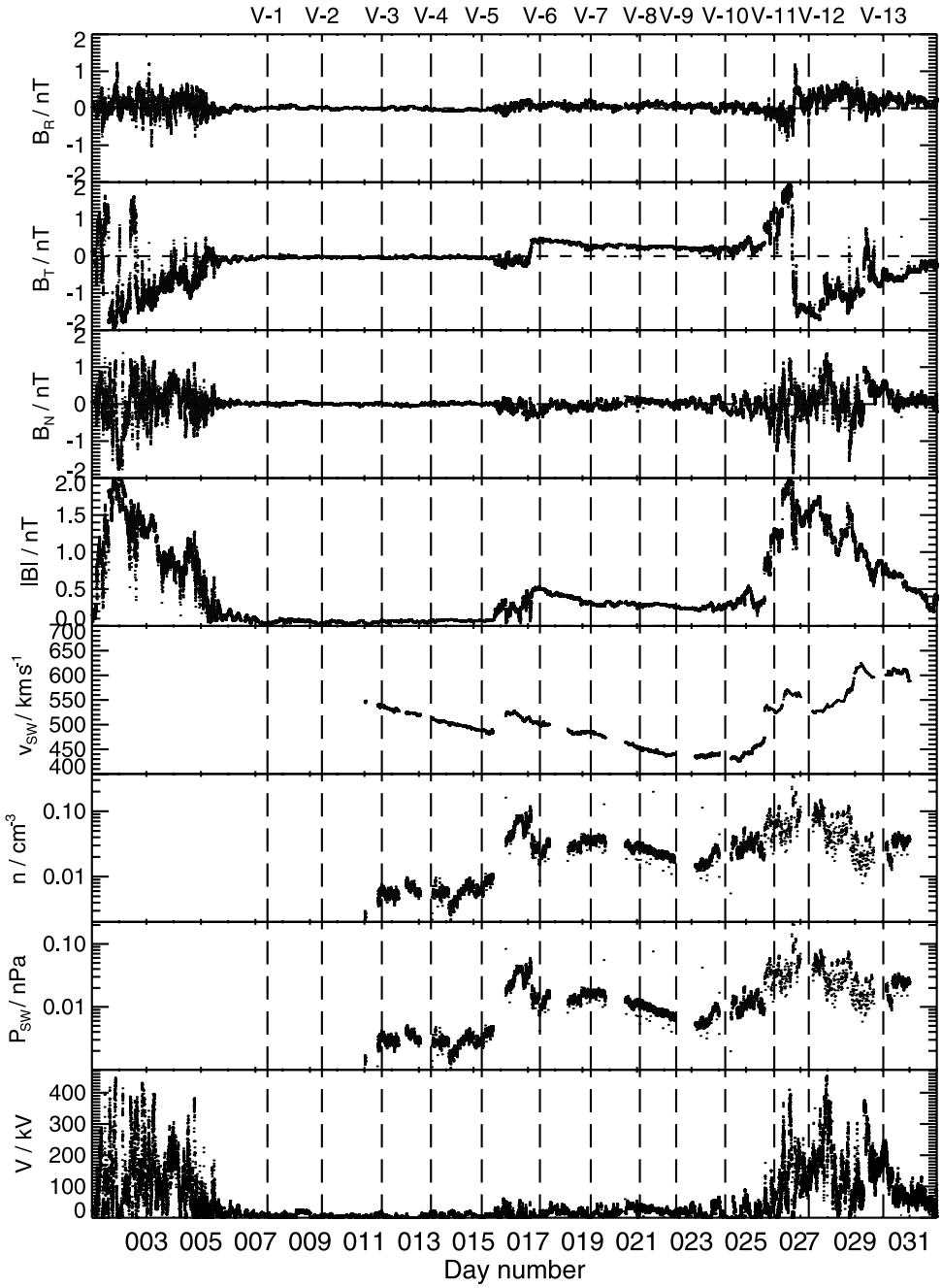

Figure 1. Upstream interplanetary conditions for the interval 1–31 January 2004 as measured by the Cassini spacecraft. The first four panels present the IMF components in RTN co-ordinates and the field magnitude. The next three panels show the solar wind velocity, density, and dynamic pressure. The final panel shows the dayside reconnection voltage estimated using the *Jackman et al.* [2004] empirical algorithm (with L_0 = 10 R_S) based on observations at Earth, as described in the text. The vertical long-dashed lines indicate the start times of the 13 visits during which the HST imaged Saturn's UV aurorae. These times have been shifted by an estimated 17 h solar wind propagation delay from Cassini to the planet, plus 68 min that the image photons took to reach HST from Saturn.

propagation effects and the difference in heliocentric longitude of Cassini and Saturn [*Crary et al.*, 2005]. In Figure 1, however, we have simply used this nominal 17 h delay, combined with the light travel delay to the HST, to indicate the start times of the HST image sequences obtained.

[10] During the January 2004 campaign a total of 68 images of Saturn's southern polar aurora were obtained by the Space Telescope Imaging Spectrograph (STIS) instrument during thirteen 'visits' by the HST, labelled 'V-1' to 'V-13' at the top of Figure 1 [*Clarke et al.*, 2005; *Grodent et al.*, 2005]. The first visit on 8 January consisted of five consecutive orbits ('V-1.1' to 'V-1.5'), designed to capture auroral variations over nearly a full planetary rotation (the start time of 'V-1.1' is indicated in Figure 1). Each subse-

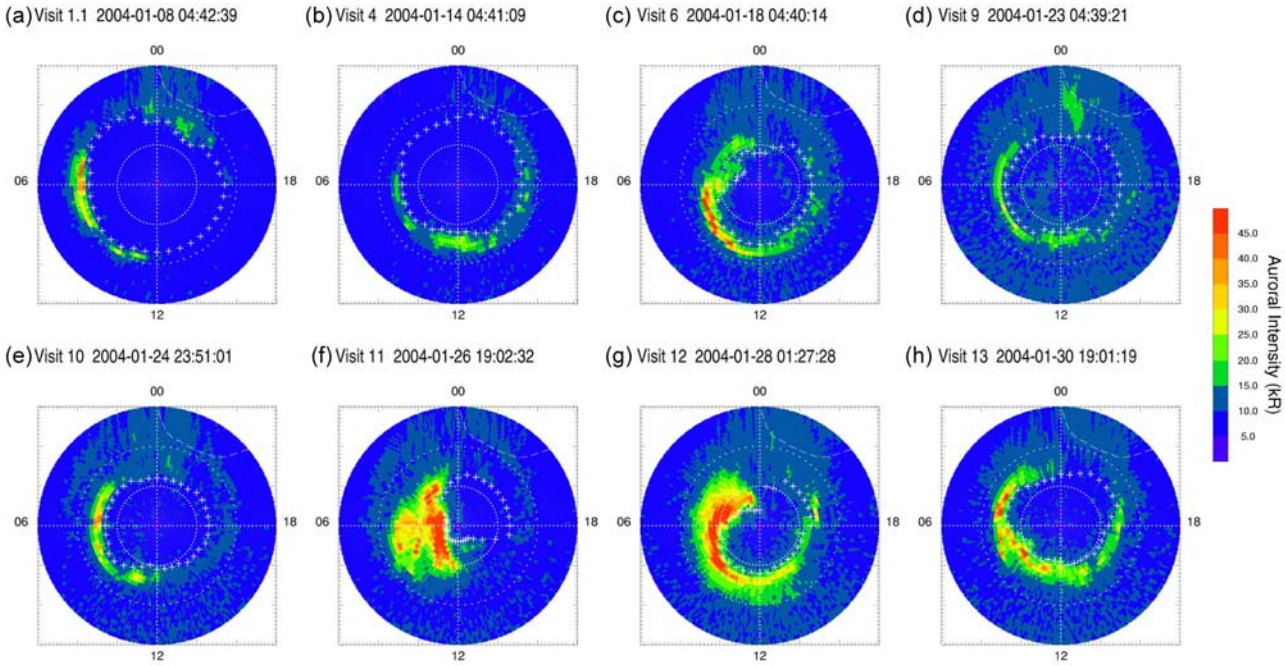

Figure 2. Selection of UV images of Saturn's southern aurora taken during January 2004, with the visit number, date, and start time of each image shown at the top of each plot. The images are projected onto a polar grid, from the pole to 30° co-latitude, viewed as though looking 'through' the planet onto the southern pole. Noon is at the bottom of each plot, and dawn to the left, as indicated. The UV auroral intensity is plotted according to the colour scale shown on the right-hand side of the figure. The white crosses mark the poleward edge of the observed auroral features as discussed in the text. The dashed white line in the pre-midnight sector marks a region of nightside emission attributed to solar UV photons scattered from Saturn's rings. The intensities shown are the average of the two unfiltered images obtained over each HST orbit.

quent visit obtained images on one orbit only. These visits were made at roughly two-day intervals as shown in Figure 1, with the last occurring on 30 January. During each orbit four UV (115–174 nm) images were obtained, the first using a SrF_2 filter to remove the Lyman-α line and potential geocoronal contamination (exposure time 640–740 s), followed by two unfiltered 'Clear' images with 270 s exposure times, and then a final filtered image. Here we have combined together the data from the two consecutive 'Clear' images on each orbit in order to increase the signal-to-noise ratio, and have then projected them onto a planetary latitude-local time grid in the manner discussed by *Gérard et al.* [2004] and *Grodent et al.* [2005]. The images view essentially the whole of the southern polar region, which was tilted significantly towards the Earth (and Sun) during the interval. A selection of the projected images is presented in Figure 2, illustrating the range of auroral behaviour observed. The data are shown on a conventional polar grid looking 'through' the planet onto the pole at the centre, with local noon at the bottom, dawn to the left, and dusk to the right. A sensitivity study performed by *Grodent et al.* [2005] has shown that the uncertainty in the mapping procedure is ~1° at the dayside but increases, mainly in latitude, to ~2° in the main auroral region on the nightside. The region from the pole to 30° co-latitude is shown, marked at intervals of 10° co-latitude. The observed UV auroral emission is colour-coded in kilo-Rayleighs (kR) according to the fixed colour scale shown on the right of the plots. The inferred poleward border of this emission is marked by white crosses, as will be discussed in the next section. A region of UV emission is also observed on the nightside which is partly composed of solar photons scattered from Saturn's rings, as well as possible auroral emissions. The region within which these ring-related emissions are observed is indicated by the white dashed line.

[11] Figure 2a was obtained on V-1.1 (8 January), and corresponds to an interval about two days after the end of the major compression region observed at the beginning of Figure 1. It shows the presence of a highly expanded oval at 15°–20° co-latitude, with brightenings in the pre-midnight, dawn, and pre-noon sector. Observations over this 'full-rotation' visit show that these features rotate around the pole with an angular velocity which is sub-corotational relative to the planet [*Clarke et al.*, 2005; *Grodent et al.*, 2005]. Figure 2b obtained on V-4 (14 January) corresponds to the first (low-field) rarefaction region, and displays a dimmer contracted oval at 12°–18° co-latitude with an auroral brightening at noon. Figure 2c obtained on V-6 (18 January) then corresponds to the interval somewhat after the arrival of the 'minor' solar wind compression at Saturn, and displays a bright contracted 'auroral spiral', running from ~5°–8° co-latitude in the post-midnight sector, through dawn, to ~13° co-latitude in the post-noon sector. It is such

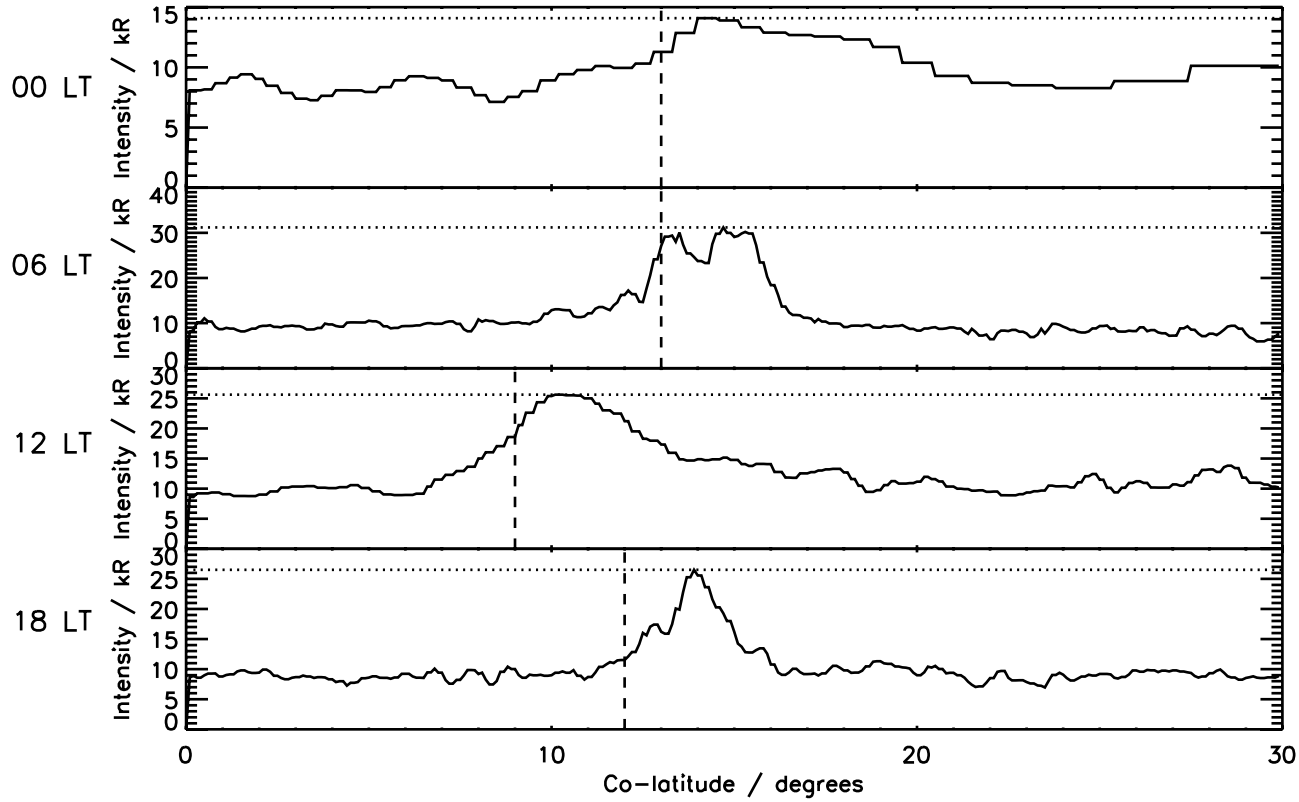

Figure 3. The intensity profile (kR) for co-latitudes 0°–30° along meridians at 0, 06, 12, and 18 MLT for visit V-13 (see Figure 2). The vertical dashed lines mark the sharp increase in auroral intensity (to the nearest 1° of co-latitude), that we have taken to indicate the poleward edge of the auroral features at each local time.

auroral structures that have been attributed by *Cowley et al.* [2005] to bursts of nightside reconnection which inject hot plasma into the sub-corotating outer magnetosphere. The next two images, Figures 2d and 2e obtained on V-9 and V-10 (23 and 24 January), respectively, correspond to the 'intermediate' rarefaction region, and show a somewhat re-expanded oval, though not to the extent of V-1.1, with auroral brightenings at dawn and noon. Figure 2f obtained on V-11 (26 January) then corresponds to the onset of the 'major' compression region, and shows a highly brightened and contracted oval, with the dawn-side almost completely 'filled-in' with bright auroral forms, from ~3° to ~15° co-latitude. About 30 h later, Figure 2g obtained on V-12 (28 January) shows that the aurorae are still bright, and have rotated into a spiral shape similar to that observed on V-6. The final image, Figure 2h obtained during V-13 (30 January), corresponds to near the end of the 'major' compression region, just over 4 days after its onset. Bright aurorae are still observed, particularly on the dawnside, and the oval has expanded somewhat to larger co-latitudes, e.g., 12°–15° co-latitude in the pre-dawn region.

2.2. Determination of the Auroral Boundary and Open Flux Estimates

[12] The selection of images in Figure 2 clearly demonstrates that the size of Saturn's auroral oval changes markedly during the Cassini-HST campaign, in response to changes in the interplanetary medium shown in Figure 1. If the central dark polar region bounded by the aurora is taken to represent the open magnetic flux region mapping to the tail lobes of the magnetosphere, on the basis of the discussion in section 1, we can then use the images to estimate the open flux present during each HST visit, and examine how it changes with time. In this section we discuss the basis on which the open flux estimates have been made.

[13] The latitudinal positions of the inferred boundary between open and closed field lines, marked by the white crosses in Figure 2, have been determined by looking for a sharp increase in the emission intensity between the polar region and the auroral zone. No specific 'cut-off' intensity has been used to determine the 'edge', since the intensity varies markedly around the boundary and between images. An example is given in Figure 3, where we show the intensity profiles versus co-latitude for 00, 06, 12, and 18 MLT for V-13, together with the inferred positions of the boundary, marked by vertical dashed lines. These are chosen to the nearest 1°, consistent with the resolution determined by the method of image projection over most of the image. For each image these positions have been determined every 10° in longitude from 0° to 350°. In regions of low intensity 'noisy' data, the boundary positions at adjacent longitudes have also been taken into account, so as to produce a boundary which is reasonably 'smooth', rather than following the detailed variations of the 'noise', which is due mainly to fluctuations in the background emission of reflected solar photons. In addition, in some local time sectors, e.g. 12–18 MLT in

Figure 2a (corresponding to V-1.1), there are no auroral features distinguishable from the background emission. In these situations the location of the boundary is estimated by simple extrapolation between the end points where the aurorae are visible, to continue a reasonable oval shape. These procedures have been applied to each of the 17 combined 'clear' images obtained during the HST-Cassini campaign, with results that can be judged from the examples provided in Figure 2.

[14] Having thus estimated the position of the poleward boundary of the aurora, we can then determine the amount of magnetic flux contained within it, taking this to be an estimate of the amount of open flux in the system according to the previous discussion. We note here, however, that it is possible that UV aurorae may also occur on open flux tubes near the dayside boundary, specifically associated with localised field-aligned currents flowing in the vicinity of the dayside cusp mapping to the magnetopause reconnection sites [*Bunce et al.*, 2005a; *Gérard et al.*, 2005]. Analysis by *Gérard et al.* [2005], for example, suggests that lobe reconnection occurring under southward IMF conditions may be the origin of a bright UV feature observed poleward of the main oval near noon in the image obtained during V-8 (not shown), corresponding to the 'intermediate' rarefaction region. If this is the case, the noon auroral 'bulge' in this image then maps to open field lines just inside the boundary, such that our procedure underestimates the amount of open flux present. Here, however, we have not attempted to take account of such features, which in the present state of understanding would require individual interpretations to be made from image to image. Instead we have maintained a consistent method, as above, within the whole sequence of images. While some uncertainty is thereby introduced, we point out that the areas of the polar cap involved, and the fluxes they contain, are small compared with the overall values. The flux within the noon 'bulge' in V-8, for example, corresponds to only ~10% of the total open flux calculated by our procedure. Positional uncertainties introduced by the method of projection also generate a maximum error of ±10% in the open flux values calculated. Uncertainties at this level will not greatly affect the conclusions reached here.

[15] To obtain the amount of open flux contained within the auroral boundary, we need to employ a model of Saturn's internal magnetic field. That employed here is the Saturn-Pioneer-Voyager (SPV) model of *Davis and Smith* [1990], determined from the near-planet Pioneer-11, and Voyager-1 and -2 magnetic data. This model is symmetric about the spin axis of the planet, and consists of aligned dipole, quadrupole, and octupole components. The field can thus be described by a flux function $F(r, \theta)$, related to the field components by $\boldsymbol{B} = (1/r \sin\theta)\,\nabla F \times \hat{\varphi}$, such that F is constant on a field line. Here we employ spherical polar co-ordinates, with r the distance from the centre of the planet, θ the co-latitude angle measured from the north pole, and φ the azimuthal angle. For the above field the flux function is [e.g., *Cowley and Bunce*, 2003b]

$$F(r,\theta) = R_S^2 \sin^2\theta \left[g_1^0 \left(\frac{R_S}{r}\right) + \frac{3}{2} g_2^0 \cos\theta \left(\frac{R_S}{r}\right)^2 + \frac{1}{2} g_3^0 \left(5\cos^2\theta - 1\right) \left(\frac{R_S}{r}\right)^3 \right], \quad (2)$$

where for the SPV model we have $g_1^0 = 21160$, $g_2^0 = 1560$, and $g_3^0 = 2320$ for a conventional Saturn radius of R_S = 60,330 km. Note that the arbitrary constant in the flux function has been chosen such that $F = 0$ at the poles. It is then readily shown that the amount of magnetic flux threading any surface bounded by a ring of radius r at co-latitude θ is $\Phi = 2\pi F(r, \theta)$. Consequently, if we divide up the area inside the auroral boundary into 36 longitudinal sectors, each $\Delta\varphi = \pi/18$ radians (i.e. 10°) wide, centred on the longitudes of the white crosses in Figure 2, then the amount of magnetic flux contained is

$$\Phi = \Delta\varphi \sum_{n=1}^{36} F(R(\theta_n), \theta_n), \quad (3)$$

where θ_n is the co-latitude of the boundary in longitude sector n, and $R(\theta_n)$ is the radius of the surface containing the auroral emissions at that co-latitude, onto which the HST data have been projected in Figure 2. This surface is assumed to be an ellipsoid of revolution about the spin axis, with an equatorial radius R_e and a polar radius R_p, i.e.,

$$R(\theta) = \frac{R_e}{(1 + \varepsilon \cos^2\theta)^{1/2}} \quad \text{where} \quad \varepsilon = \left(\frac{R_e}{R_p}\right)^2 - 1. \quad (4)$$

The surface containing the peak auroral emissions lies 1000 km above the 1 bar reference spheroid of the planet for the unfiltered images, such that R_e = 61268 km ≈ 1.02 R_S, R_p = 55364 km ≈ 0.92 R_S, and $\varepsilon \approx 0.22$ [*Trauger et al.*, 1998; *Grodent et al.*, 2005].

3. Magnetospheric Dynamics During the January 2004 Cassini-HST Campaign

[16] Using the algorithm defined by equations (2) to (4), we can compute the amount of flux contained within the auroral boundary, representing our estimate of the open flux in Saturn's magnetosphere, for each of the HST images. In this section we now present our results for the interval, and discuss how the changing amount of open flux relates to concurrent interplanetary conditions.

3.1. Variation of the Open Flux

[17] In Figure 4 the open flux estimates obtained for each of the combined 'Clear' images are shown in the bottom panel by the crosses joined by solid lines, plotted versus time. The times shown are the start times of the intervals in which the observed aurora actually occurred at Saturn, i.e. the HST time minus 68 min. The stars and dashed lines in this panel show the corresponding values of the power in UV auroral emissions from H_2 and H, extrapolated from the STIS bandpass over the range covering the H_2 Lyman and Werner bands using a synthetic emission spectrum [*Clarke et al.*, 2005; *Grodent et al.*, 2005]. The uncertainties in these values are estimated to be about ±15%. The relationship to the interplanetary data is indicated in the top two panels, where we show the solar wind dynamic pressure and IMF magnitude, respectively. These data have been shifted forward in time by the estimated 17-h propagation delay to match the image times, such that the relative timing of the HST and Cassini data remains identical to Figure 1 (which

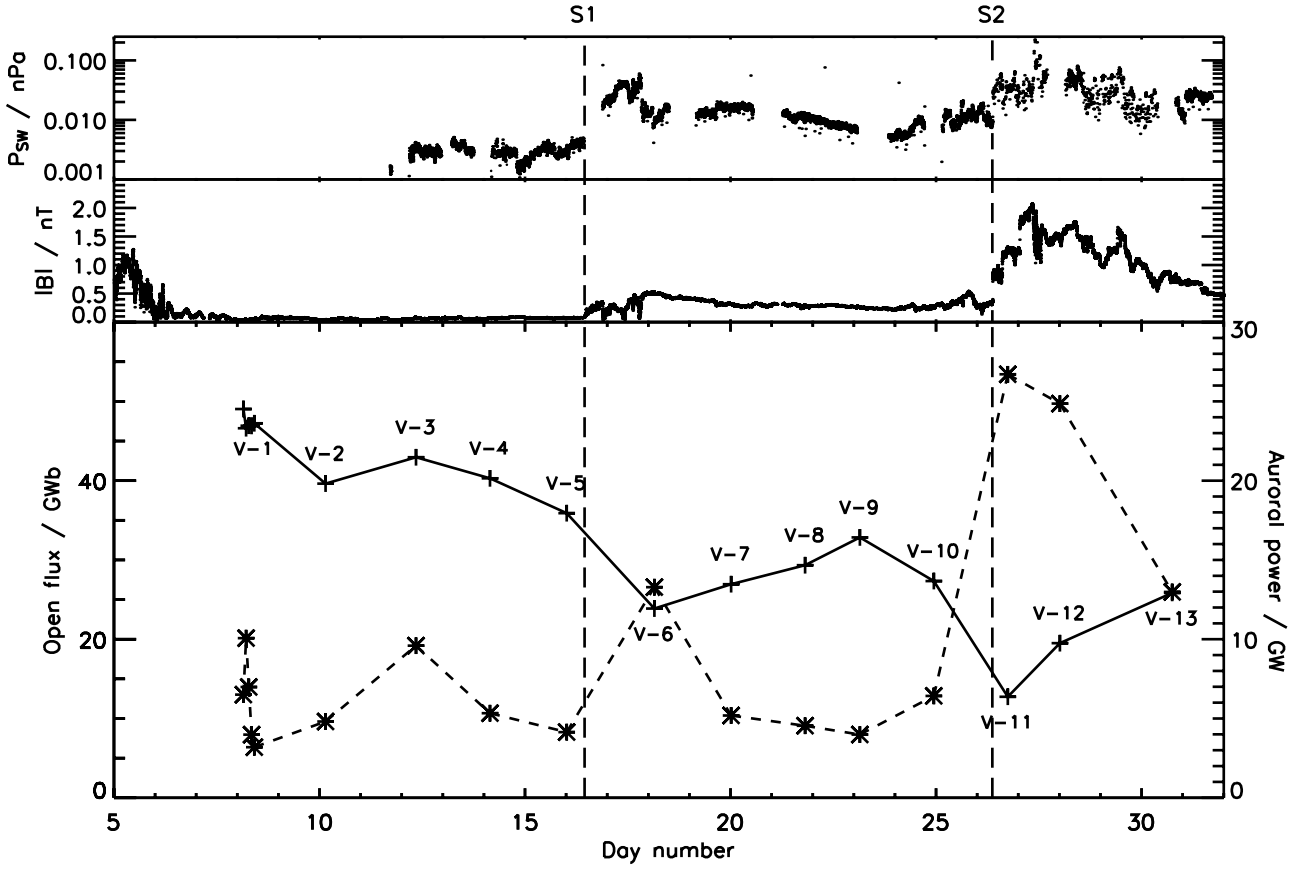

Figure 4. The open flux content of the southern polar cap estimated from the HST images is plotted versus time in the bottom panel, shown by the crosses marked at each HST visit (V-1 to V-13) and joined by the solid line. The times marked are the actual times the aurora occurred at Saturn, i.e. the HST time minus 68 min. Also shown by the stars and dashed line are the values of the power in UV auroral emissions from H_2 and H at each visit (using the right-hand scale), extrapolated from the STIS bandpass over a wavelength range covering the H_2 Lyman and Werner bands using a synthetic emission spectrum. The top and middle panels show the solar wind dynamic pressure and interplanetary magnetic field strength, respectively, measured by the Cassini spacecraft for 1–31 January 2004 and shifted forward by the 17 h propagation delay to match the times the aurora occurred. The vertical dashed lines mark the estimated arrival times of two solar wind shocks marking the start of CIR-related compressions.

focused on Cassini data and hence employed Cassini measurement times). The two vertical dashed lines in the plot show the (shifted) times of the forward shocks which initiated the minor (S1) and major (S2) CIR-related compressions, indicated by the sudden increases in field strength. The shifted times of arrival at Saturn occurred on days 16 and 26 respectively. The tail-end of the previous 'major' compression region starting on day 1, prior to the HST imaging interval, can also be seen at the beginning of the plot.

[18] The sequence of images begins with the most expanded auroral oval observed during the interval, this being the image from V-1.1 shown in Figure 2a. The open flux contained within the oval in this case is estimated to be 49 GWb. Over the five orbits of V-1, corresponding to an interval of ~7 h on day 8, *Grodent et al.* [2005] show that the auroral morphology changed significantly, associated with sub-corotation of major auroral features at ~65% of the planetary rotation rate. The overall auroral power also varied significantly, between ~5 and ~10 GW, as can be seen in Figure 4. Nevertheless, the open flux deduced from the five independent images varies by only ~5%, between ~47 and ~49 GWb, thus indicating that our method is reasonably robust, and does not lead to major scatter in the open flux values. This near-constant flux result is also consistent with modest reconnection rates occurring during the interval, as might be expected from the rarefaction region conditions then prevailing. However, to produce a clearly observable effect over this short interval, say a change in open flux of more than ~5 GWb in either direction, the average net reconnection rate would have to exceed ~200 kV.

[19] Two days later, however, on day 10, the open flux estimated from the V-2 image is clearly smaller at ~40 GWb, the value then remaining relatively steady for V-3 and V-4 (Figure 2b), varying by only ~3 GWb. Following this on day 16, the V-5 image indicates that the open flux content had decreased further to 36 GWb. All these images were obtained during the initial low-field solar wind rarefaction interval, during which magnetopause

reconnection rates are predicted to be very low [*Jackman et al.*, 2004; *Bunce et al.*, 2005a]. These results indicate the occurrence of an interval of variable net open flux closure within Saturn's magnetosphere associated with tail reconnection, as will be quantified in the following section. Visit V-5 occurred a few hours before the arrival at the planet of the forward shock (S1) of the minor compression region. The effects of this are seen prominently in the next measurement on V-6 (Figure 2c), which occurred ~1.5 days after the projected arrival of the compression. From the V-6 image we deduce an open flux of ~24 GWb, suggesting that ~12 GWb of flux was closed in the 2 days between V-5 and V-6. There is also a significant increase in the auroral power recorded at V-6, rising from a value of a few GW to ~13 GW. *Cowley et al.* [2005] have suggested that such events are associated with compression-induced intervals of major open flux closure in Saturn's magnetic tail.

[20] Visits V-7 to V-10 (Figures 2d and 2e) then occurred during the solar wind rarefaction region of intermediate field strength on days 20–24. The first three of these images indicate a steady increase in the size of the auroral oval, with the open flux rising to ~33 GWb at V-9. This indicates the occurrence of an interval of net accumulation of open flux in the tail due to magnetopause reconnection. On V-10 (Figure 2e), however, the open flux content reduced again to ~27 GWb, indicating the excitation of tail reconnection. The auroral power correspondingly showed a small increase from 4–5 GW during V-7 to V-9, up to ~6.5 GW during V-10. The major solar wind compression initiated by shock S2 then arrived at Saturn during day 26, associated with substantial effects ~9 h later in the image obtained on V-11 (Figure 2f). This displays the smallest polar cap observed in this sequence, containing only ~13 GWb of open flux, together with the highest auroral power observed of ~27 GW. The net flux closure between V-10 and V-11 is thus estimated to be ~15 GWb. During the final two visits, V-12 and V-13 (Figures 2g and 2h), the open flux then increased again while the auroral power declined, this indicating an interval of net open flux production in the presence of enhanced compression-region interplanetary field strengths. The final open flux estimate obtained on V-13 was ~26 GWb, with an auroral power of ~13 GW. We note that as a whole, the interval shown in Figure 4 is associated with falling values of the open flux, the initial value being almost twice as large as the final. Given the recurrent nature of interplanetary conditions over each ~25 day solar rotation during this period [*Jackman et al.*, 2004], however, we may expect that the condition of Saturn's magnetosphere should also be approximately cyclical over a complete solar rotation. Therefore we anticipate that had observations been made in the interval following V-13, the open flux content would have increased back towards values seen during V-1 (i.e. to ~45–50 GWb), the latter being observed ~2 days after the end of the preceding major solar wind compression which occurred one solar rotation earlier.

[21] To summarise these observations, significant decreases in the open flux were observed following major compressions of the magnetosphere by the solar wind between V-5 and V-6, and V-10 and V-11, by ~12 and ~15 GWb, respectively. These intervals are thus inferred to be associated with rapid net closure of open flux in the magnetospheric tail produced by solar wind compressions of Saturn's magnetosphere, in agreement with the previous discussions of *Jackman et al.* [2004] and *Cowley et al.* [2005]. After these decreases, the open flux then increased again over several days due to net open flux production in the relatively high-field strength intervals that followed. Decreases in open flux were also observed during the first low-field solar wind rarefaction region interval, with an overall reduction of ~13 GWb between V-1 and V-5, and at the end of the intermediate rarefaction region, where a reduction of ~6 GWb occurred between V-9 and V-10. These observations are suggestive of the occurrence of intermittent intervals of more modest net tail reconnection, as discussed by *Grodent et al.* [2005] and *Bunce et al.* [2005a]. We also observe in Figure 4 a general anti-correlation between the amount of open flux contained in the polar cap (i.e. the size of the auroral oval) and the auroral power, in agreement with the results presented previously by *Clarke et al.* [2005]. This suggests a relationship between auroral luminosity and intervals of tail reconnection and open flux closure, similar to that observed at Earth [e.g., *Milan et al.*, 2005].

3.2. Magnetopause and Tail Reconnection Rate Estimates

[22] The variations in open flux shown in Figure 4 provide a measure of the difference between the rates at which open flux is produced at Saturn's magnetopause and destroyed in the tail. If we can make a quantitative estimate of the rate of open flux production at the magnetopause from the upstream solar wind conditions we can compare this to the open flux estimates made above and hence also estimate average tail reconnection rates. This then enables discussion of the overall open flux throughput in the system during the interval of HST observations.

[23] Given the current level of understanding of the reconnection process, it is not possible to calculate the reconnection rate ab initio. Instead, studies at the Earth have developed empirical formulae based on simple theoretical ideas, which are fitted to available data. These formulae have been applied to Saturn's magnetosphere by *Jackman et al.* [2004] after taking into account the opposite polarity of Saturn's magnetic field and the different scale size of the magnetosphere. Specifically, *Jackman et al.* [2004] suggest that the rate of open flux production at Saturn's magnetopause, equal to the voltage along the magnetopause reconnection region, can be estimated from the following empirical relation

$$V = v_{SW} B_{\perp} L_0 \cos^4(\theta/2), \tag{5}$$

where v_{SW} is the radial solar wind velocity, $B_{\perp}$ is the magnitude of the IMF vector perpendicular to the radial flow, and θ is the 'clock angle' of this vector measured from the planet's north magnetic axis projected onto the T-N plane (in RTN coordinates). The open flux production rate according to this formula is therefore at a maximum when the IMF points north ($\theta = 0°$), and reduces to zero when it points south ($\theta = 180°$), opposite to the case of the Earth due to the opposite polarity of the planetary field. Parameter L_0 in equation (5) is a scale length which is equal, when $\theta = 0°$, to the width of the solar wind channel, perpendicular to the $\boldsymbol{B}_{\perp}$ vector, in which the IMF reconnects with the planetary

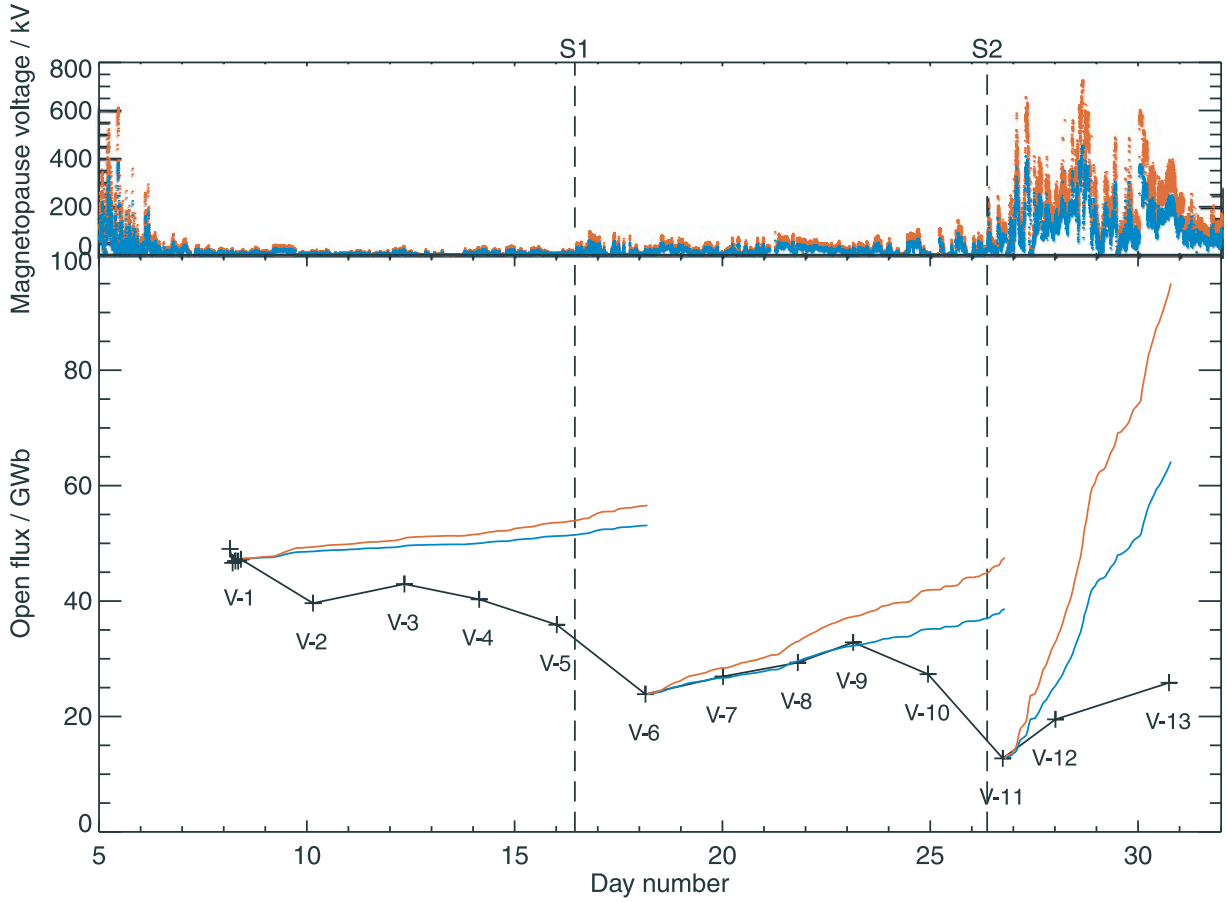

Figure 5. The open flux content of the southern polar cap is shown in the lower panel by black crosses joined by the solid black line, as in Figure 4. The upper panel presents the magnetopause reconnection voltages estimated from the upstream interplanetary Cassini data using the *Jackman et al.* [2004] empirical algorithm (see text) with L_0 = 10 R_S (blue) or 16 R_S (red). The blue and red lines in the lower panel show the corresponding accumulation of open flux in the system, obtained by integrating the magnetopause voltages over time, assuming no tail reconnection occurs. As in Figure 4, the vertical dashed lines mark the estimated arrival times of two solar wind shocks marking the start of CIR-related compressions.

field. *Jackman et al.* [2004] estimated its value by scaling the empirically-determined corresponding length at Earth by the respective size of the planetary magnetosphere, specifically by the radius of the subsolar magnetopause. *Milan et al.* [2005] found L_0 at Earth to lie in the range 5 – 8 R_E, where R_E is Earth's radius, compared with a subsolar magnetopause radius of ~10 R_E. At Saturn, the radius of the subsolar magnetopause is ~20 R_S [e.g., *Behannon et al.*, 1983], thus suggesting the value of L_0 to lie in the range 10–16 R_S. *Jackman et al.* [2004] employed the specific value L_0 = 10 R_S, which has been used to derive the magnetopause reconnection voltages (open flux production rates) from equation (5) shown in the bottom panel of Figure 1. (Note that in intervals where no solar wind velocity data are available, we simply used the velocity value nearest in time to calculate the voltage. During days 1–11, for example, we used a constant value of 550 km s^{-1}, representing a reasonable typical value.) Generally, the voltage values follow the modulation of the IMF strength, though with considerable structure superposed through rapid variations in the clock angle, on time scales down to a few tens of minutes. These voltages vary from very small values, ~10 kV or less, during the weak field rarefaction region, to peaks of ~400 kV within the major compressions.

[24] Integration of the magnetopause reconnection voltages over time then allows us to estimate the open flux produced over given intervals, and hence the expected accumulation of open flux in the system if tail reconnection is zero. This is shown in the lower panel of Figure 5. Here the crosses joined by black lines show the open flux values obtained from the HST images as in Figure 4, while the coloured lines show the expected growth in open flux obtained by integrating the estimated magnetopause reconnection voltages. The latter voltages estimated from the Cassini data are shown for reference in the upper panel (with the same time shift as in Figure 4), where the blue and red dots correspond to L_0 = 10 and 16 R_S, respectively. The blue and red lines in the lower panel then show the corresponding cumulative integrals of these voltage values. On the left of the figure these lines have been initialised at the open flux value obtained from averaging the five

measurements made on V-1, i.e., 47 GWb, such that they show the open flux that would be present versus time if no tail reconnection occurred after V-1. The difference between these lines and the black line at a given time then provides an estimate of the open flux that has been closed in the tail since V-1. The coloured lines are then re-initialised following the auroral contraction events, and major flux closures, observed on V-6 and V-11.

[25] During the first rarefaction region, low magnetopause reconnection rates of a few tens of kV are estimated due to the low IMF field strength, such that the amount of open flux produced over the interval is small. Over the whole ~8-day interval between V-1 and V-5 the open flux produced is estimated to be only ~4–6 GWb. (In this section parameter ranges correspond to taking L_0 = 10–16 R_S unless otherwise indicated.) If no tail reconnection occurred, we would then expect the open flux present at V-5, at the end of the rarefaction interval, to be ~51–54 GWb as shown. By comparison, the open flux deduced from the V-5 image is ~36 GWb, indicating that ~15–18 GWb had been closed in the tail since V-1. The implied tail reconnection rate is ~23–27 kV averaged over the whole interval, though the intermediate HST images suggest that the rate of closure is not constant, but is large, for example, in the interval between V-1 and V-2, and weak between V-2 and V-3.

[26] The open flux then decreases significantly between V-5 and V-6, associated with the first (S1) solar wind compression, thus implying a large increase in the tail reconnection rate. Taking account also of the open flux estimated to be produced in the interval, the total amount of open flux which is closed between these visits is estimated to be ~14–15 GWb, corresponding to an averaged tail reconnection rate of ~75–81 kV. The instantaneous rates could, of course, be significantly higher. After the compression, the re-initialised coloured lines in Figure 5 show that open flux should accumulate more rapidly than before due to the stronger fields present in the intermediate field-strength rarefaction region that follows, where voltage values peak at ~100 kV as seen in the upper panel. The observed increase in open flux inferred from the HST images between V-6 and V-9 closely follows the predicted value for L_0 = 10 R_S (blue line), consistent with essentially zero tail reconnection during the interval, while the values for L_0 = 16 R_S (red line) indicate an overall flux closure of ~5 GWb during this interval associated with a weak averaged tail reconnection rate of ~10 kV. The open flux inferred from the V-10 image, however, falls well below both coloured lines, indicating averaged tail reconnection rates towards the end of the rarefaction region interval, between V-9 and V-10, of ~54–65 kV.

[27] Again taking account of the estimated open flux production, the total open flux inferred to be closed between V-10 and V-11, associated with the second (S2) compression, is then ~18–20 GWb, resulting in an estimated averaged tail reconnection rate of ~117–130 kV over the interval. After this, the open flux production rates are very large, associated with the strong fields and large magnetopause voltages in the compression region, such that the coloured lines in the lower panel of Figure 5 increase much more steeply than before. From a re-initialised value of 13 GWb at V-11, the open fluxes reach values of 64 and 95 GWb (for the blue and red lines respectively) by the end of the image sequence on 30 January. The open flux values inferred from the HST images at V-12 and V-13 are significantly lower than this, however, at 20 and 26 GWb respectively, indicating that as well as the very high magnetopause reconnection rates, averaging ~141–226 kV over the interval, there is also a comparable (but slightly lower) reconnection rate in the tail. These observations indicate a system which is strongly driven by the reconnection-mediated solar wind interaction during this 4-day interval.

[28] Our results on reconnection rates during the interval of HST observations are summarised and systematised in Figure 6. The top panel again shows the (time-shifted) magnetopause reconnection rates estimated from the Cassini data in the same format as in Figure 5, such that the blue and red dots correspond to L_0 = 10 and 16 R_S in equation (5), respectively. The blue and red columns in the second panel then show these values averaged over the intervals between each HST visit, as indicated by the visit numbers shown. The third panel displays the solar wind dynamic pressure in the same format as in Figure 4. The bottom panel then shows the corresponding values of the tail reconnection rate averaged between each visit, inferred from the change in open flux observed in the HST images, combined with the open flux production estimate shown above.

[29] It can be seen that during the low-field, low-pressure rarefaction region between V-1 and V-5, the magnetopause reconnection rates are very low, averaging ~6–10 kV. The corresponding tail reconnection rates are very variable, between essentially zero and ~60 kV, but average to ~23–27 kV as indicated above, such that overall the open flux in the system slowly declines. (We note that the small negative tail voltage values inferred during the interval between V-2 and V-3 are of course unphysical, and provide a measure of the uncertainties involved).

[30] The arrival of the first (S1) solar wind compression between V-5 and V-6 results in a small increase in the average magnetopause reconnection voltage to 10–16 kV, while the averaged tail reconnection rate jumps to 75–81 kV. In the intermediate field strength rarefaction region that follows, encompassing V-6 to V-10, the averaged magnetopause voltages remain somewhat elevated at ~20–30 kV. The tail reconnection rates are then essentially zero between V-6 and V-9, leading to a slow but steady accumulation of open flux in the system, before increasing to 54–65 kV between V-9 and V-10, similar to the peak tail voltages inferred in the initial rarefaction region between V-1 and V-2.

[31] The arrival of the second (S2) solar wind compression in the interval between V-10 and V-11 again signals a major enhancement in the averaged tail reconnection rate to 117–130 kV, while the averaged magnetopause rate is initially only marginally increased. Due to the strong fields in the following compression region, however, the averaged magnetopause rate then increases very markedly, to peak at values of ~162–260 kV between V-12 and V-13. The inferred tail reconnection rates also peak at 135–233 kV during this interval, though remain less than the dayside rates, such that overall the open flux slowly increases.

3.3. Relationship of Reconnection Rates and Auroral Morphology

[32] The results obtained above suggest that a variety of physical scenarios were observed in the HST images during

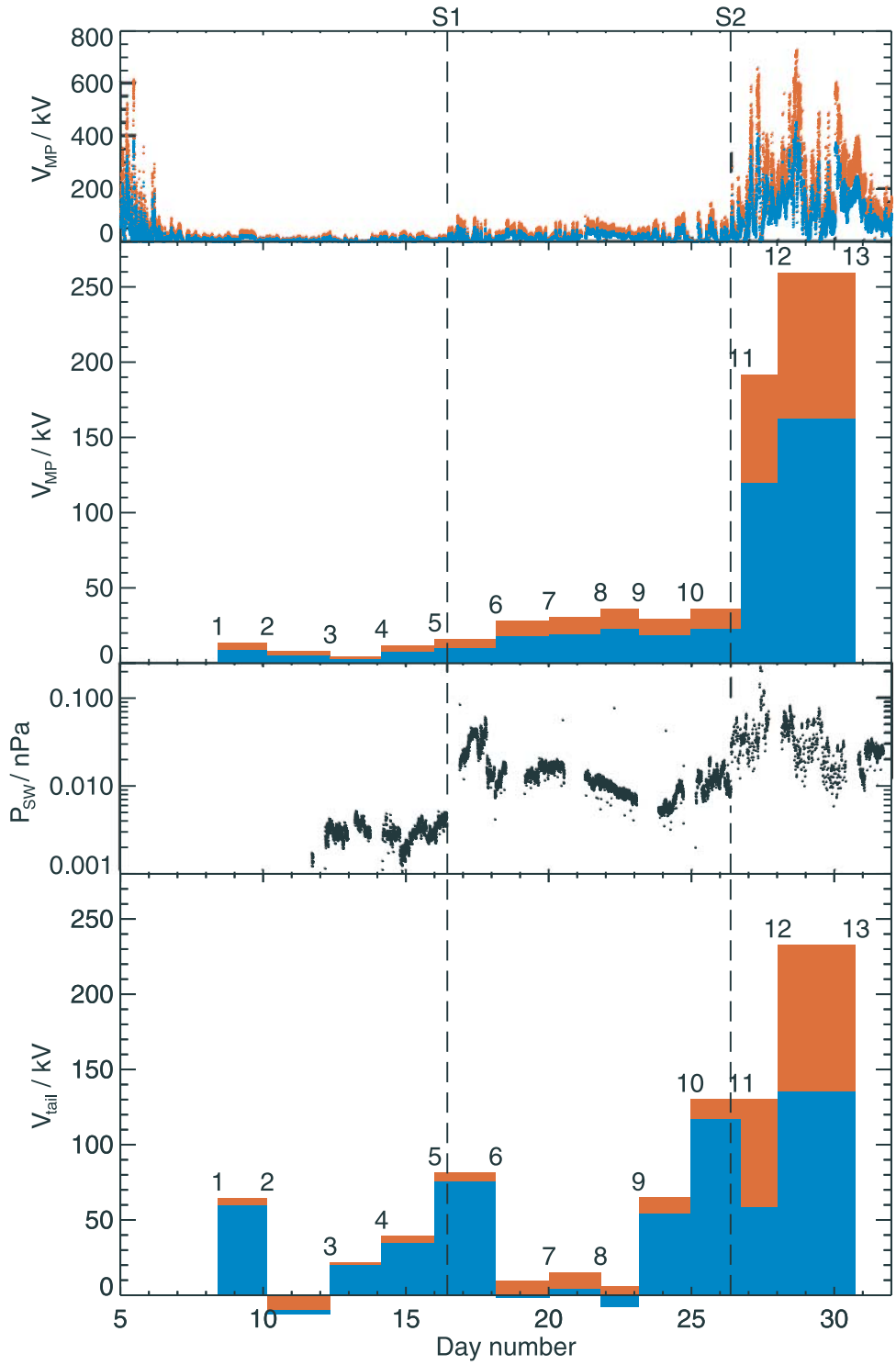

Figure 6. Averaged magnetopause and tail reconnection voltages for the intervals between the HST images. The top panel displays the estimated magnetopause reconnection voltages at 1 min resolution according to the *Jackman et al.* [2004] algorithm with L_0 = 10 R_S (blue) or 16 R_S (red), as in Figure 5. The red and blue columns in the second panel show these voltages averaged over the intervals between successive HST images, the times of which are marked by the visit numbers 1 to 13. The third panel displays the solar wind dynamic pressure derived from Cassini measurements over the interval. The red and blue columns in the bottom panel show the corresponding averaged tail reconnection voltages, derived by combining the averaged magnetopause reconnection voltages in the second panel with the net change in open flux over the intervals determined from the HST images.

the January 2004 campaign, including intervals of intermittent tail reconnection and small magnetopause reconnection rate during V-1 to V-5, intermittent magnetopause reconnection and small tail reconnection rate during V-7 to V-9, large tail reconnection during V-6 and V-11, and large tail and magnetopause reconnection combined in V-12, V-13, and possibly V-10. It is now of interest to re-examine the auroral distributions themselves in the light of these results. *Cowley et al.* [2004a, 2005] have described how the auroral emissions expected at Saturn are produced from two sources of precipitation, which give rise to 'discrete' and 'diffuse' aurora respectively. Discrete aurorae are associated with regions of upward-directed field-aligned current located at and near the open-closed field line boundary, which are sufficiently intense to require the downward acceleration of magnetospheric electrons into the atmosphere. Diffuse aurorae, located equatorward of the boundary on closed field lines, are formed by the precipitation into the atmosphere of hot magnetospheric plasma produced principally by tail dynamics, which is trapped on closed flux tubes, and which generally sub-corotates around the outer magnetosphere from its nightside source. *Cowley et al.* [2004a] initially discussed steady-state conditions, while *Cowley et al.* [2005] considered the features expected in various non-steady reconnection scenarios. A selection of their results pertinent to our discussion is presented in Figure 7. These show sketches of the plasma flow (short-dashed arrowed lines), field-aligned currents (circled dots and crosses representing upward and downward flow respectively), and regions of diffuse precipitation (stippled regions) in Saturn's polar ionosphere, viewed looking down onto the pole with the sunward direction at the bottom and dawn to the left, as in Figure 2. The solid line in these diagrams also marks the boundary between open and closed field lines, with active reconnection sites being represented by long-dashed lines terminated by the X symbols.

[33] Figure 7a shows the conditions expected for an ongoing few-hour burst of tail reconnection in the absence of magnetopause reconnection. A 'bulge' of diffuse emission intrudes into the polar cap on newly-closed flux tubes on the nightside, and extends into a growing dawn-side spiral 'tail' on closed field lines in the downstream flow. An intense bipolar pair of field-aligned currents also flows within the bulge, forming a system similar to the substorm current wedge at Earth. The current is directed upward on the dawn side of the bulge, giving enhanced 'discrete' precipitation in this sector, and extends into enhanced upward currents and discrete aurorae in the dawn boundary region, excited by the enhanced Dungey-cycle flow of closed flux returning to the dayside via dawn. If such reconnection occurs over many hours, comparable to the ~20 h sub-corotation time around the planet in the outer magnetosphere, then the aurora will form a spiral pattern extending from the nightside bulge via dawn to noon and beyond. Following *Cowley et al.* [2005], we suggest that such a pattern corresponds to that observed during V-6 shown in Figure 2c, where in section 3.2 above we inferred the occurrence of strong compression-induced tail reconnection (~80 kV averaged over two days) in the absence of strong magnetopause reconnection (~10 kV similarly averaged). V-11 (Figure 2f) is then suggested to correspond to a more extreme version of such a bulge (also compression-induced) imaged early in its formation.

[34] If, on the other hand, the tail reconnection is intermittent on a time scale which is short compared with the sub-corotation time, the process will result instead in the creation of diffuse auroral 'patches' which sub-corotate around the outer magnetosphere, mapping to the region just equatorward of the open-closed field line boundary, as shown in Figure 7b. In this case the polar cap is shown to have regained its equilibrium (near-circular) shape, and the Dungey-cycle flows have ceased, such that there is no longer a dawn enhancement of the boundary currents and discrete aurorae. Following *Grodent et al.* [2005], we suggest that this scenario relates to conditions during the first rarefaction region where we have inferred the presence of intermittent tail reconnection (two-day averaged between ~0 and ~60 kV) in the absence of significant magnetopause reconnection (typically averaging less than 10 kV). The image obtained during V-1.1 shown in Figure 2a, for example, may represent an auroral patch observed shortly (a few hours) after its formation, while that obtained during V-4 (Figure 2b) shows a patch that has rotated over several hours into the noon sector. In general, patches may be observed at any local time in this case.

[35] Conditions expected for an interval of dayside reconnection in the absence of tail reconnection are shown in Figure 7c. In this case the process does not result in an enhancement of diffuse emissions on closed field lines, but still produces a response in the field-aligned currents and discrete aurorae. Specifically, there will now be an intense bipolar current system at noon associated with the reconnection region, as recently discussed by *Bunce et al.* [2005a], with enhanced upward field-aligned currents again extending around the dawn boundary region from noon. These currents will lead to a related enhancement of discrete aurorae at dawn compared with dusk, now most prominently expressed in the dayside region. According to the above results these conditions apply to the intermediate rarefaction region observed during V-7 to V-9, at least intermittently when the IMF pointed northwards. Magnetopause reconnection rates during the interval average to ~20–30 kV, with typically less than ~10 kV of tail reconnection. The aurorae in these cases generally show an enhancement at dawn compared with dusk, such as that shown for V-9 shown in Figure 2d, with a variable morphology in the vicinity of noon which may relate to IMF-dependent cusp emission [*Gérard et al.*, 2005].

[36] Finally, Figure 7d illustrates conditions when significant magnetopause and tail reconnection are both in progress over many hours. In this case bipolar field-aligned currents are present in both magnetopause and tail reconnection regions, extending into enhanced upward boundary currents and discrete aurora at dawn. A diffuse auroral spiral also winds from the nightside hours around the boundary via dawn to noon and possibly beyond. The form of the spiral is expected to depend somewhat on the relative rates of magnetopause and tail reconnection prevailing. If the magnetopause reconnection rate is higher than that in the tail (over several hours), then the spiral will be truncated in the noon sector as outer magnetosphere flux tubes are opened at the magnetopause and transferred to the tail. If, on the other hand, the tail reconnection rate is greater than the magnetopause rate, as illustrated in Figure 7d, then a reduced spiral will continue past noon into the dusk sector.

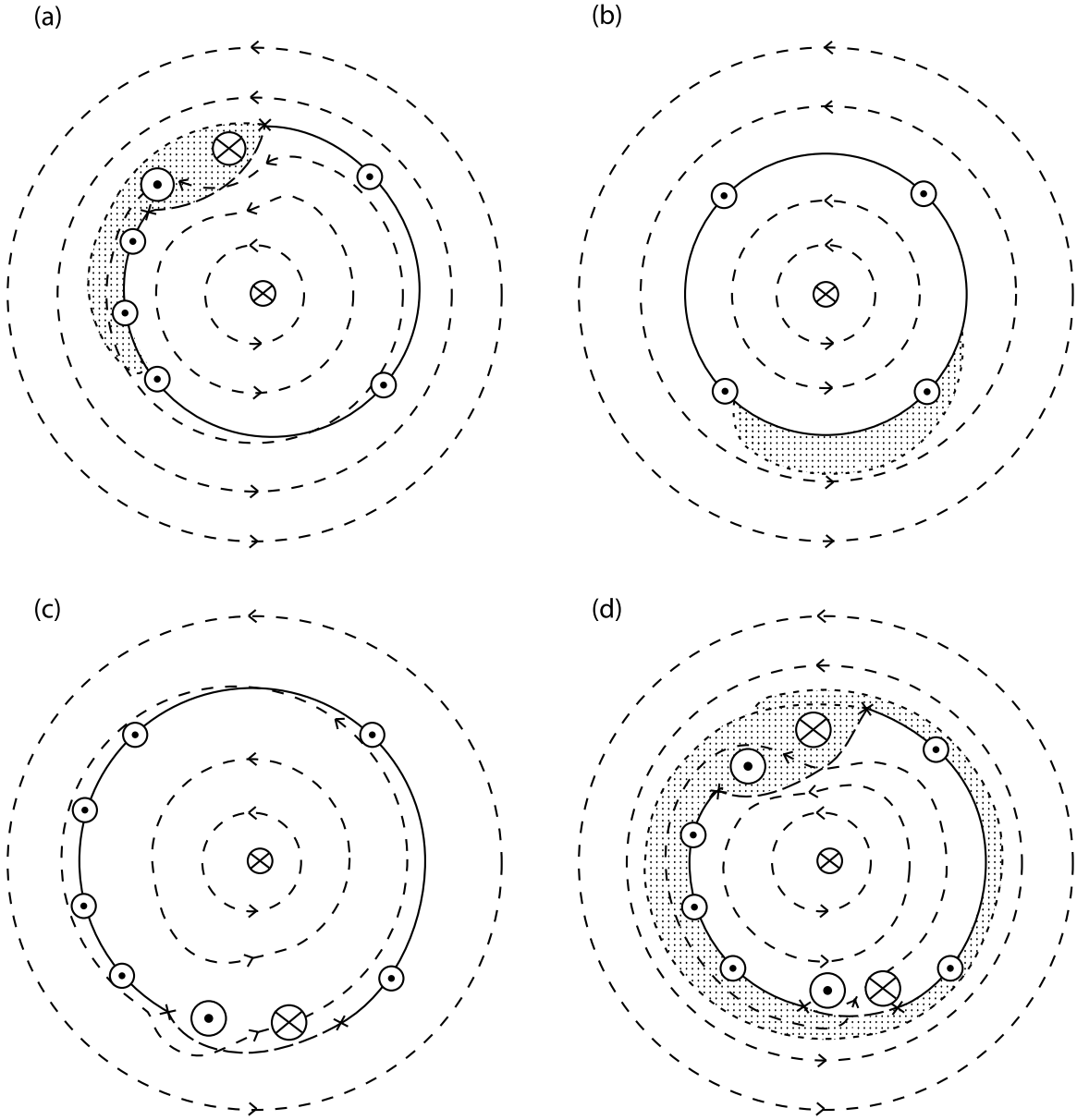

Figure 7. Sketches of the plasma flow, field-aligned currents, and diffuse precipitation regimes in Saturn's polar ionosphere. Noon is at the bottom of each diagram, dawn to the left, and dusk to the right (as for the HST UV auroral images shown in Figure 2). The outermost circle corresponds to a co-latitude $\sim 30^\circ$ from the pole. The arrowed short-dashed lines show plasma streamlines, while the long-dashed lines marked by crosses represent active reconnection lines associated with the Dungey cycle. The solid line marks the boundary between open and closed field lines. Circled dots and crosses represent upward and downward field-aligned currents, respectively. Their relative intensity is roughly denoted by the size of the symbol. Stippling indicates regions of hot plasma precipitation along closed field lines. The figure s represent conditions for (a) an on-going few-hour burst of tail reconnection, (b) a sub-corotating auroral patch formed by a few-hour burst of tail reconnection, (c) an on-going burst of dayside reconnection, and (d) an extended interval of concurrent tail and dayside reconnection.

However, since magnetopause reconnection is often rather intermittent on hour time scales due to fluctuations in the IMF direction, the latter may represent the more general case, with a narrowed and variable spiral remaining in the post-noon sector. We suggest that this scenario applies to the aurorae observed in V-12 and V-13 shown in Figures 2g and 2h, where our results indicate the presence of both strong reconnection at the magnetopause and in the tail with comparable averaged rates of $\sim 100-200$ kV, where the spiral appears to become dimmer, narrower, and/or more intermittent in the post-noon sector. We suggest that the scenario also applies to V-10 shown in Figure 2e, where we have also inferred the presence of comparable tail (~ 50 kV) and magnetopause (~ 30 kV) reconnection rates averaged over the preceding interval, though the rates are significantly less than for V-12 and V-13. In this case bright auroral

emissions at dawn are truncated in a bright possibly cusp-related auroral spot in the pre-noon sector.

[37] Overall, it seems reasonable to conclude from these results that the observed auroral morphologies are at least qualitatively consistent with expectations based on the inferred magnetopause and tail reconnection rates, according to the picture presented by *Cowley et al.* [2005].

4. Summary

[38] In this paper we have considered the data obtained during the Cassini-HST Saturn campaign in January 2004. Data from the Cassini spacecraft obtained in the interplanetary medium upstream of Saturn show that two CIR-related solar wind compressions were observed during the interval, on days 16 and 26, characterised by high field strengths and velocities, surrounded by several-day low-field rarefaction regions [*Jackman et al.*, 2004; *Crary et al.*, 2005; *Bunce et al.*, 2005b]. Such structured solar wind conditions are typical of the declining phase of the solar cycle so although the data described here is limited in duration, it should be representative of significant periods of each solar cycle. HST images of Saturn's southern UV aurora obtained during the interval show strong variations in morphology related to these upstream conditions [*Clarke et al.*, 2005; *Grodent et al.*, 2005]. Using the poleward edge of the aurora as a proxy for the open-closed field line boundary, the open flux content in the polar cap has been estimated for each set of images and has been found to vary markedly between 13 and 49 GWb, thus indicating significant magnetosphere-solar wind interactions during the interval. The magnetopause reconnection voltage (open flux production rate) was also calculated from the upstream conditions using the algorithm proposed by *Jackman et al.* [2004], and integrated over time to estimate the amount of open flux created at the magnetopause in the ($\sim$2 day) intervals between the HST images. Comparison with the open flux values inferred from the HST images themselves then also allows us to estimate the tail reconnection voltage (the rate of open flux closure), averaged over the interval between the images. The observed auroral morphologies have also been related to the reconnection rates derived, and discussed in relation to the theoretical picture presented by *Cowley et al.* [2005].

[39] The results are summarised as follows. During an extended rarefaction interval of very low interplanetary field strength and consequent very low magnetopause reconnection rate (typically <10 kV), we infer the presence of intermittent bursts of flux closure in the tail, averaging up to $\sim$60 kV over $\sim$2 days, which produces irregular sub-corotating auroral patches that can be observed at any local time. In a rarefaction region of intermediate field strength where the magnetopause reconnection voltages were larger, on average 20–30 kV, but the tail reconnection rates were small over an extended interval (<10 kV), the auroral forms were typically enhanced at dawn and have variable morphologies at noon, taken to be related to the excitation of Dungey-cycle flow and cusp precipitation, respectively. A burst of tail reconnection (averaging $\sim$50 kV) also occurred at the end of the latter rarefaction interval, further increasing the brightness of the dawn emission. CIR-related solar wind compressions induce strong tail reconnection and net open flux closure, characterised by 2-day averaged reconnection voltages of $\sim$70–140 kV. These intervals are associated with bright auroral features in the pre-dawn sector that develop into spiral forms over time. In the extended high-field strength interval that followed the onset of one of the solar wind compressions, both tail and magnetopause reconnection voltages were inferred to be enhanced to averaged values of $\sim$150–250 kV. The aurorae observed during the interval are spiral forms with intense emissions in the pre-dawn to noon sector, and lesser emissions post-noon. The observations are thus in reasonable qualitative agreement with expectations based on the theoretical picture presented by *Cowley et al.* [2005].

[40] Overall our results suggest that reconnection in Saturn's tail can be initiated in two distinct ways. First, it can be initiated during relatively quiet solar wind intervals, possibly by moderate solar wind events which are not CIR compression-related [e.g., *Lyons et al.*, 1997] or by some internal instability triggered when the open flux exceeds a certain threshold. For example, the tail flux increased steadily between V-6 and V-9 without evidence of significant tail reconnection, before tail reconnection began between V-9 and V-10. It seems possible that such events are similar to substorms at Earth. Evidence for 'substorm'-like activity in Saturn's tail has recently been presented by *Mitchell et al.* [2005], using data from the MIMI instrument on Cassini. Second, larger flux closures can be triggered by the sudden major magnetospheric compressions associated with interplanetary shocks. These events are also known at Earth but are relatively rare compared with ordinary substorms. Their significance at Saturn is enhanced by the generally long time-scales required for the growth of open flux in the tail, several days rather than an hour or two, such that the time-scale for 'substorms' becomes comparable with the interval between CIR-related shock compressions. In either case, bright aurorae would tend to be associated with intervals of reduced open flux, thus giving rise to the observed anti-correlation between these parameters.

[41] Although our study is limited by the availability of data, it leads to a series of general conclusions that can be addressed using Cassini data. Perhaps the most interesting is the conclusion that tail dynamics can occur intermittently during quiet interplanetary conditions, as well as being initiated by interplanetary compression events. These conclusions should be directly testable using Cassini in situ and remote sensing data. Fuller understanding of auroral morphologies and their relation to interplanetary conditions and Saturn's magnetospheric dynamics, however, will require further joint Cassini-HST studies in the future.

[42] **Acknowledgments.** Work at Leicester was supported by PPARC grant PPA/G/O/2003/00013. E.J.B. was supported by PPARC Post-Doctoral Fellowship PPA/P/S/2002/00168. J.C.G. and D.G. were supported by the Belgian Fund for Scientific Research (FNRS). This work employs observations made by the NASA/ESA Hubble Space Telescope, obtained at the Space Telescope Science Institute, which is operated by the AURA Inc for NASA. We thank F. J. Crary and the CAPS instrument team for use of the solar wind velocity data employed to calculate the voltage values used in this study. CAPS is supported by a contract with NASA/JPL.

[43] Arthur Richmond thanks Michel Blanc and Athanasios Boudouridis for their assistance in evaluating this paper.

References

Behannon, K. W., R. P. Lepping, and N. F. Ness (1983), Structure and dynamics of Saturn's outer magnetosphere and boundary regions, *J. Geophys. Res.*, *88*, 8791.

Boudouridis, A., E. Zesta, L. R. Lyons, P. C. Anderson, and D. Lummerzheim (2003), Effect of solar wind pressure pulses on the size and strength of the auroral oval, *J. Geophys. Res.*, *108*(A4), 8012, doi:10.1029/2002JA009373.

Boudouridis, A., E. Zesta, L. R. Lyons, P. C. Anderson, and D. Lummerzheim (2004), Magnetospheric reconnection driven by solar wind pressure fronts, *Ann. Geophys.*, *22*, 1367.

Broadfoot, A. L., et al. (1981), Extreme ultraviolet observations from Voyager 1 encounter with Saturn, *Science*, *212*, 206.

Bunce, E. J., S. W. H. Cowley, and S. E. Milan (2005a), Interplanetary magnetic field control of Saturn's polar cusp aurora, *Ann. Geophys.*, *23*, 1405.

Bunce, E. J., S. W. H. Cowley, C. M. Jackman, J. T. Clarke, F. J. Crary, and M. K. Dougherty (2005b), Cassini observations of the interplanetary medium upstream of Saturn and their relation to Hubble Space Telescope auroral data, *Adv. Space Res.*, in press.

Clarke, J. T., H. W. Moos, S. K. Atreya, and A. L. Lane (1981), IUE detection of bursts of H Ly α emission from Saturn, *Nature*, *290*, 226.

Clarke, J. T., et al. (1998), Hubble Space Telescope imaging of Jupiter's UV aurora during the Galileo orbiter mission, *J. Geophys. Res.*, *103*(E9), 20,217.

Clarke, J. T., et al. (2005), Morphological differences between Saturn's ultraviolet aurorae and those of Earth and Jupiter, *Nature*, *433*, 717.

Cowley, S. W. H., and E. J. Bunce (2001), Origin of the main auroral oval in Jupiter's coupled magnetosphere-ionosphere system, *Planet. Space Sci.*, *49*, 1067.

Cowley, S. W. H., and E. J. Bunce (2003a), Modulation of Jupiter's main auroral oval emissions by solar wind-induced expansions and compressions of the magnetosphere, *Planet. Space Sci.*, *51*, 57.

Cowley, S. W. H., and E. J. Bunce (2003b), Corotation-driven magnetosphere-ionosphere coupling currents in Saturn's magnetosphere and their relation to the auroras, *Ann. Geophys.*, *21*, 1691.

Cowley, S. W. H., et al. (2003), Solar wind-magnetosphere-ionosphere interactions in the Earth's plasma environment, *Philos. Trans. A*, *361*, 113.

Cowley, S. W. H., E. J. Bunce, and R. Prangé (2004a), Saturn's polar ionospheric flows and their relation to the main auroral oval, *Ann. Geophys.*, *22*, 1379.

Cowley, S. W. H., E. J. Bunce, and J. M. O'Rourke (2004b), A simple quantitative model of plasma flows and currents in Saturn's polar ionosphere, *J. Geophys. Res.*, *109*, A05212, doi:10.1029/2003JA010375.

Cowley, S. W. H., S. V. Badman, E. J. Bunce, J. T. Clarke, J.-C. Gérard, D. Grodent, C. M. Jackman, S. E. Milan, and T. K. Yeoman (2005), Reconnection in a rotation-dominated magnetosphere and its relation to Saturn's auroral dynamics, *J. Geophys. Res.*, *110*, A02201, doi:10.1029/2004JA010796.

Crary, F. J., et al. (2005), Solar wind dynamic pressure and electric field as the main factors controlling Saturn's auroras, *Nature*, *433*, 720.

Davis, L., Jr., and E. J. Smith (1990), A model of Saturn's magnetic field based on all available data, *J. Geophys. Res.*, *95*, 15,257.

Desch, M. D. (1982), Evidence for solar wind control of Saturn radio emission, *J. Geophys. Res.*, *87*, 4549.

Desch, M. D., and H. O. Rucker (1983), The relationship between Saturn kilometric radiation and the solar wind, *J. Geophys. Res.*, *88*, 8999.

Dungey, J. W. (1961), Interplanetary field and the auroral zones, *Phys. Rev. Lett.*, *6*, 47.

Gérard, J.-C., V. Dols, D. Grodent, J. H. Waite, G. R. Gladstone, and R. Prangé (1995), Simultaneous observations of the saturnian aurora and polar haze with the HST/FOC, *Geophys. Res. Lett.*, *22*, 2685.

Gérard, J.-C., D. Grodent, J. Gustin, A. Saglam, J. T. Clarke, and J. T. Trauger (2004), Characteristics of Saturn's FUV aurora observed with the Space Telescope Imaging Spectrograph, *J. Geophys. Res.*, *109*, A09207, doi:10.1029/2004JA010513.

Gérard, J.-C., E. J. Bunce, D. Grodent, S. W. H. Cowley, J. T. Clarke, and S. V. Badman (2005), Signature of Saturn's auroral cusp: Simultaneous HST FUV observations and upstream solar wind monitoring, *J. Geophys. Res.*, *110*, A11201, doi:10.1029/2005JA011094.

Grodent, D., J. T. Clarke, J. Kim, J. H. Waite Jr., and S. W. H. Cowley (2003), Jupiter's main auroral oval observed with HST-STIS, *J. Geophys. Res.*, *108*(A11), 1389, doi:10.1029/2003JA009921.

Grodent, D., J.-C. Gérard, S. W. H. Cowley, E. J. Bunce, and J. T. Clarke (2005), The global morphology of Saturn's southern ultraviolet aurora, *J. Geophys. Res.*, *110*, A07215, doi:10.1029/2004JA010983.

Hill, T. W. (1979), Inertial limit on corotation, *J. Geophys. Res.*, *84*, 6554.

Hill, T. W. (2001), The jovian auroral oval, *J. Geophys. Res.*, *106*, 8101.

Jackman, C. M., N. Achilleos, E. J. Bunce, S. W. H. Cowley, M. K. Dougherty, G. H. Jones, S. E. Milan, and E. J. Smith (2004), Interplanetary magnetic field at ~9 AU during the declining phase of the solar cycle and its implications for Saturn's magnetospheric dynamics, *J. Geophys. Res.*, *109*, A11203, doi:10.1029/2004JA010614.

Judge, D. L., F. M. Wu, and R. W. Carlson (1980), Ultraviolet photometer observations of the Saturnian system, *Science*, *207*, 431.

Kurth, W. S., et al. (2005), An Earth-like correspondence between Saturn's auroral features and radio emission, *Nature*, *433*, 722.

Lyons, L. R., G. T. Blanchard, J. C. Samson, R. P. Lepping, T. Yamamoto, and T. Moretto (1997), Coordinated observations demonstrating external substorm triggering, *J. Geophys. Res.*, *102*, 27,039.

McGrath, M. A., and J. T. Clarke (1992), H I Lyman alpha emission from Saturn (1980–1990), *J. Geophys. Res.*, *97*, 13,691.

Meurant, M., J.-C. Gérard, C. Blockx, B. Hubert, and V. Coumans (2004), Propagation of electron and proton shock-induced aurora and the role of the interplanetary magnetic field and solar wind, *J. Geophys. Res.*, *109*, A10210, doi:10.1029/2004JA010453.

Milan, S. E., M. Lester, S. W. H. Cowley, K. Oksavik, M. Brittnacher, R. A. Greenwald, G. Sofko, and J.-P. Villain (2003), Variations in polar cap area during two substorm cycles, *Ann. Geophys.*, *21*, 1121.

Milan, S. E., S. W. H. Cowley, M. Lester, D. M. Wright, J. A. Slavin, M. Fillingim, C. W. Carlson, and H. J. Singer (2004), Response of the magnetotail to changes in the open flux content of the magnetosphere, *J. Geophys. Res.*, *109*, A04220, doi:10.1029/2003JA010350.

Milan, S. E., J. A. Wild, A. Grocott, and N. C. Draper (2005), Space- and ground-based investigations of solar wind-magnetosphere-ionosphere coupling, *Adv. Space Res.*, in press.

Mitchell, D. G., et al. (2005), Energetic ion acceleration in Saturn's magnetotail: Substorms on Saturn?, *Geophys. Res. Lett.*, *32*, L20S01, doi:10.1029/2005GL022647.

Ness, N. F., M. H. Acuña, R. P. Lepping, J. E. P. Connerney, K. W. Behannon, L. F. Burlaga, and F. M. Neubauer (1981), Magnetic field studies by Voyager 1: Preliminary results at Saturn, *Science*, *212*, 211.

Nichols, J. D., and S. W. H. Cowley (2004), Magnetosphere-ionosphere coupling currents in Jupiter's middle magnetosphere: Effect of precipitation-induced enhancement of the ionospheric Pedersen conductivity, *Ann. Geophys.*, *22*, 1799.

Prangé, R., D. Rego, L. Pallier, J. E. P. Connerney, P. Zarka, and J. Queinnec (1998), Detailed study of FUV jovian auroral features with the post-COSTAR HST faint object camera, *J. Geophys. Res.*, *103*, 20,195.

Prangé, R., L. Pallier, K. C. Hansen, R. Howard, A. Vourlidas, R. Courtin, and C. Parkinson (2004), An interplanetary shock traced by planetary auroral storms from the Sun to Saturn, *Nature*, *432*, 78.

Sandel, B. R., and A. L. Broadfoot (1981), Morphology of Saturn's aurora, *Nature*, *292*, 679.

Sandel, B. R., et al. (1982), Extreme ultraviolet observations from the Voyager 2 encounter with Saturn, *Science*, *215*, 548.

Shemansky, D. E., and J. M. Ajello (1983), The Saturn spectrum in the EUV: Electron excited hydrogen, *J. Geophys. Res.*, *88*, 459.

Southwood, D. J., and M. G. Kivelson (2001), A new perspective concerning the influence of the solar wind on Jupiter, *J. Geophys. Res.*, *106*, 6123.

Trauger, J. T., et al. (1998), Saturn's hydrogen aurora: Wide field and planetary camera 2 imaging from the Hubble Space Telescope, *J. Geophys. Res.*, *103*, 20,237.

Vasyliunas, V. M. (1983), Plasma distribution and flow, in *Physics of the Jovian Magnetosphere*, edited by A. J. Dessler, p. 395, Cambridge Univ. Press, New York.

S. V. Badman, E. J. Bunce, S. W. H. Cowley, and S. E. Milan, Department of Physics and Astronomy, University of Leicester, Leicester LE1 7RH, UK. (svb4@ion.le.ac.uk)

J. T. Clarke, Department of Astronomy, Boston University, 725 Commonwealth Avenue, Boston, MA 02215, USA.

J.-C. Gérard and D. Grodent, LPAP, Université de Liège, Allée du 6 Août – Sart Tilman, B4000 Liège, Belgium.